Tetrahedron Letters 173 (2025) 155830

Contents lists available at ScienceDirect

Tetrahedron Letters

journal homepage: www.elsevier.com/locate/tetlet

Dual-type photodynamic therapy enabled by fluorinated BODIPY-liposome hybrids for enhanced antibacterial efficacy

Zhihua Chen [a], Jincheng Zhu [b], Mengxing Wang [b], Qinglin Wu [a], Yichun Xu [c,*], Lei Cui [b,*], Kewen Zheng [a,*]

[a] School of Environmental and Chemical Engineering, Shanghai University, Shanghai 200444, China
[b] College of Science, Shanghai University, Shanghai 200444, China
[c] Department of Pathology, Shanghai Tongji Hospital, Tongji Hospital Affiliated to Tongji University, Shanghai 200065, China

ARTICLE INFO

Keywords:
Boron-dipyrromethene
Photosensitizers
Photodynamic therapy
Liposomes

ABSTRACT

The widespread misuse of antibiotics has accelerated bacterial evolution, precipitating a global antimicrobial resistance (AMR) crisis. Photodynamic therapy (PDT) has recently emerged as a promising alternative due to its non-invasiveness, cost-effectiveness and broad-spectrum antimicrobial activity. Boron-dipyrromethene (BODIPY) derivatives constitute a promising class of organic photosensitizers with experimentally verified photodynamic activity. However, conventional BODIPY-based photosensitizers face significant limitations: their inherent hydrophobicity reduces reactive oxygen species (ROS) generation efficiency, diminishes antimicrobial coverage, and may paradoxically promote resistance development. Furthermore, their exclusive production of Type I PDT, without complementary Type II mechanisms, substantially restricts their therapeutic potential. Herein, a series of photosensitizers (PSs) with antibacterial properties was developed by leveraging electron push-pull systems coupled with heavy-atom effects. In addition to enhance the aqueous solubility of photosensitizers, three types were encapsulated into liposomes via the thin film hydration method. Benefiting from sufficient molecular rotors and high electronegativity of fluorine, the developed BDP-F Lips exhibit superior ROS generation capacity under laser irradiation, concurrently producing both Type I and Type II PDT, thereby demonstrating excellent antibacterial efficacy.

Introduction

Global public health faces escalating antimicrobial challenges as antibiotic misuse and rapid pathogen evolution drive precipitous declines in conventional antibiotic efficacy. The World Health Organization has declared antimicrobial resistance (AMR) "one of the most urgent public health threats of the 21st century" [1–5]. Conventional antibacterial approaches now confront substantial limitations, necessitating urgent development of novel antimicrobial agents to address the burgeoning bacterial infection crisis.

Currently, researchers have developed several novel antibacterial approaches such as phage therapy [6–8], antimicrobial peptides [9–11], and photodynamic therapy [12]. Among these, photodynamic therapy exhibits distinct advantages: superior broad-spectrum efficacy, precision targeting, rapid action, and biosafety [13]. An ideal photosensitizer (PS) for photodynamic antimicrobial applications should possess the following characteristics: strong visible-light absorption capacity, reversible redox potential, long electron lifetime, prolonged excited triplet-state lifetime, significant photoluminescence quantum yield coupled with high triplet-state energy, and facile structural modifiability for tuning photophysical properties and catalytic efficiency [14]. BODIPY dyes have successfully addressed these challenges by virtue of their intense visible-light absorption, high fluorescence quantum yield, exceptional photochemical stability, and thermal stability, establishing their efficacy as potent photosensitizers. The most salient feature of BODIPY lies in the facile functionalization of its core structure at α, β, and *meso* positions, enabling custom-tailored designs for diverse applications [15]. This characteristic enables precise modulation of the compound's photophysical and electro-chemical properties, facilitating the development of a wide range of BODIPY derivatives. These derivatives demonstrate broad application prospects in fluorescence imaging, photodynamic therapy, functionalized materials, optoelectronics, and photocatalysis. However, conventional BODIPY derivatives exhibit limited aqueous solubility, which restricts their

* Corresponding authors.
E-mail addresses: crystalxyc@hotmail.com (Y. Xu), cuilei@shu.edu.cn (L. Cui), zhengkw@shu.edu.cn (K. Zheng).

https://doi.org/10.1016/j.tetlet.2025.155830
Received 6 July 2025; Received in revised form 12 September 2025; Accepted 16 September 2025
Available online 18 September 2025

applicability. Furthermore, the overwhelming majority of PSs for PDT preferentially undergo the Type II energy transfer pathway between the excited triplet state and proximate molecular oxygen to generate singlet oxygen ($^1O_2$). This process is inherently constrained by high oxygen consumption rates. Many researchers are addressing these issues, such as Zhen et al. [16], who encapsulated photosensitizers into liposomes via the thin-film hydration method to enhance biocompatibility. Wang et al. [17] developed two photosensitizers, QY1 and QY2, based on symmetric A-DA'D-A and asymmetric A-DA'D-A" configurations. These molecules both feature a ladder-type core (DA'D) fused with an electron-deficient benzothiadiazole unit at the center and 4,5,6,7-Tetrabromo-1,3-indanedione side units. Under red-light irradiation, QY1 and QY2 simultaneously generated complementary Type-I ROSs of •OH and $O_2^{\bullet-}$. The former possesses strong oxidizing ability, while the latter exhibits a long lifetime. Based on the above considerations, a photo-therapeutic agent design strategy emerged by introducing heavy atoms into the indene ring to construct π-extended conjugated molecular skeletons. Heavy atoms incorporated into the indene moiety simultaneously promote the intersystem crossing (ISC) process, thereby increasing the triplet state population of PSs to enhance ROS generation efficiency. Herein, three PSs with F, Cl and Br atom substitutions on the indene ring were designed and subsequently encapsulated into liposomes to improve biocompatibility. Subsequent ROS assays demonstrated their capacity for concurrent generation of both type I and type II ROS with sustained production capability. Consequently, antibacterial tests were conducted, revealing that BDP-F Lips exhibit exceptional efficacy against Gram-positive E.coli, consistent with the ROS assay results.

Results and discussion

Synthesis and characterization

The precursor BODIPY core and three halogen-substituted indene rings have been previously reported [17,18]. As detailed in Scheme 1, BDP-F, BDP-Cl, and BDP-Br were successfully synthesized. Initially, BDP was reacted with p-Anisaldehyde via the Knoevenagel reaction to afford BDP-1. Subsequently, BDP-1 underwent the Vilsmeier reaction to yield BDP-2. Finally, BDP-2 was subjected to the Knoevenagel reaction to generate various BDP derivatives bearing heavy-atom substituents (see Scheme 2). The structural charact-erization details of these novel compounds are provided in the Supporting Information.

Photophysical properties and theoretical calculations

Photophysical properties of BODIPY derivatives with different heavy-atom substituents were investigated. As shown in Fig. 1, the three photosensitizers exhibited nearly identical maximum UV absorption peaks at 614 nm, 619 nm and 620 nm, respectively. This minimal shift

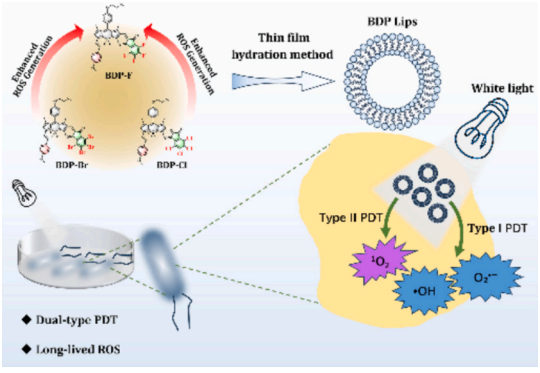

Scheme 1. Schematic showing the chemical structure of PSs (BDP-F, BDP-Cl, and BDP-Br) and BDP-F Lips for PDT-based synergistic therapy.

may be attributed to similar conjugation extension effects imparted by halogens, resulting in insignificant variations in absorption maxima. Despite differing electronegativities and atomic radii of F, Cl, and Br, these auxochromes primarily induce bathochromic shifts through lone-pair electron conjugation with the chromophore (n-π* transitions). As congeners, their capacity for lone-pair electron conjugation may be insufficient to significantly alter the electronic transition energy of the main chromophore. Alternatively, given that the absorption peaks arise primarily from π-π* transitions (as opposed to n-π* transitions or other lone-pair-sensitive transitions), halogen substitution is likely to induce only minor modifications to transition energies through inductive effects, without causing significant shifts in absorption maxima. The maximum fluorescence emission peaks of the three photosensitizers were similarly proximate at 650 nm, 658 nm, and 654 nm. Emission wavelengths are primarily determined by transitions from the lowest vibrational level of the first excited singlet state to the ground state, and F/Cl/Br substituents exert minimal influence on the energy levels of the core chromophore, thus yielding comparable emission maxima. The brominated derivative exhibited the most red-shifted emission, potentially due to synergistic effects of hyper-conjugation, polarizability, and excited-state structural relaxation.

To enhance the water solubility of the photosensitizers, three liposomes were prepared using the thin-film hydration method. The particle sizes of BDP-F Lips, BDP-Cl Lips and BDP-Br Lips in aqueous solution were measured by dynamic light scattering (DLS). As depicted in Fig.S15 (ESI†), the average hydrodynamic diameters of BDP-F Lips, BDP-Cl Lips, and BDP-Br Lips were 145.4 nm, 217.9 nm, and 188.0 nm, respectively, all falling within the typical liposome size range (100–500 nm). The homogeneous lipid bilayer structure facilitates stable encapsulation and controlled release of photosensitizers, thereby enhancing the Enhanced Permeability and Retention (EPR) effect while reducing nonspecific tissue distribution. Transmission electron microscopy (TEM) images revealed well-defined sizes and uniform morphological structures for all three liposomes, demonstrating their successful preparation. The UV–vis and fluorescence spectra of the liposomal photosensitizers exhibited principal spectral features closely matching those of the photosensitizers, indicating that encapsulation within liposomes did not alter their photophysical properties, thus confirming the successful preparation of the liposomal formulations.

To elucidate the electronic properties of these photosensitizers (PS), density functional theory (DFT) calculations at the B3LYP/6-31G(d) level were performed using Gaussian software to determine the molecular geometries and frontier molecular orbitals of BDP-1, BDP-F, BDP-Cl and BDP-Br. This yielded the electron density distributions and energy levels of the highest occupied molecular orbital (HOMO) and lowest unoccupied molecular orbital (LUMO). As shown in Fig. 2, the LUMO electron density encompasses the terminal capping group of the Br-Indene moiety, whereas the HOMO lacks such distribution. This observation indicates an intramolecular charge transfer (ICT) characteristic in the excited state of BDP-F, BDP-Cl and BDP-Br, which facilitates bathochromic shifting of emission peaks into the near-infrared region. Compared to BDP-1, chemical modification enhances electron delocalization across the molecular framework, facilitating intramolecular electron transfer. The calculated HOMO and LUMO energy levels were: BDP-1 (−4.88 eV, −2.40 eV), BDP-F (−5.25 eV, −2.89 eV), BDP-Cl (−5.29 eV, −2.94 eV), and BDP-Br (−5.25 eV, −2.89 eV), respectively (Fig.S16, ESI†). The closely aligned energy levels across all three photosensitizers are consistent with their previously analyzed photophysical properties. Their band gaps (2.48 eV, 2.36 eV, 2.35 eV, 2.36 eV) are narrower than those of several established photosensitizers. This reduced band gap not only promotes excited-state electron transfer for efficient ROS generation via Type I or Type II photochemical pathways but also enables oxygen-independent ROS production, thereby diminishing oxygen dependency and enhancing photodynamic efficacy. Subsequently, time-dependent DFT (TD-DFT) calculations revealed ΔE_{ST} values of 1.26 eV, 1.03 eV, 0.99 eV and 0.99 eV for BDP-F, BDP-Cl and

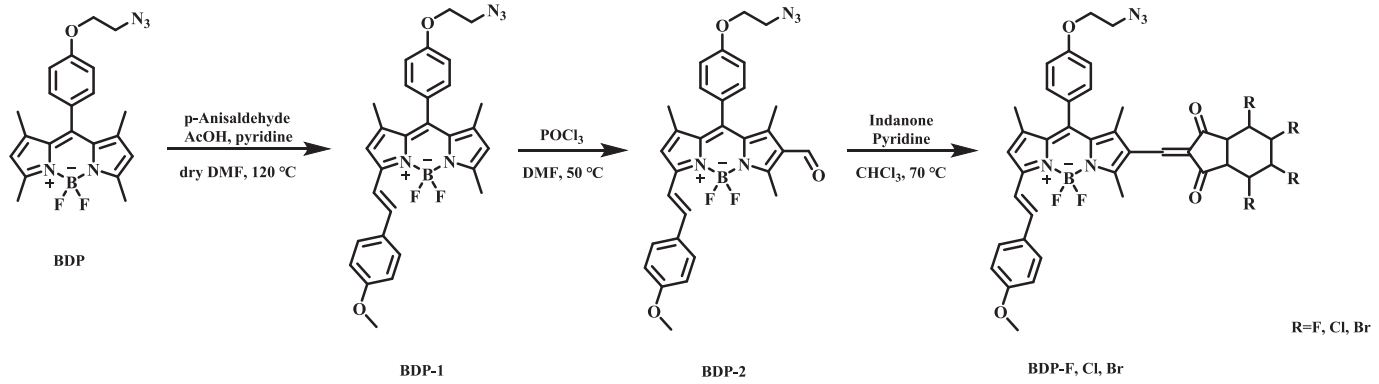

Scheme 2. Synthesis of BDP-F, BDP-Cl, and BDP-Br.

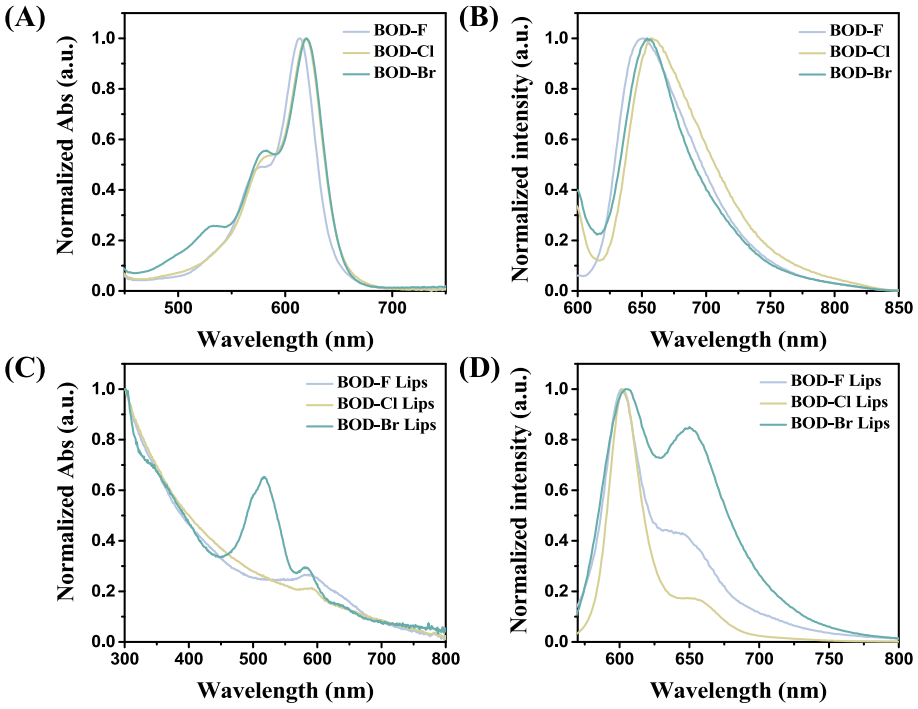

Fig. 1. A) Absorption and B) fluorescence spectra of BDP-F, BDP-Cl and BDP-Br. C,D) The optical spectral characteristics in the water of BDP-F Lips, BDP-Cl Lips and BDP-Br Lips (1×10^{-5} M).

BDP-Br, respectively (Fig.S17, ESI†). Comparative analysis with BDP-1 reveals that the chemically modified photosensitizer exhibits a reduced ΔE_{ST}, which facilitates triplet exciton generation via enhanced intersystem crossing (ISC) efficiency. This process augments electron transfer capacity, thereby significantly promoting reactive oxygen species (ROS) generation.

ROS generation in aqueous solvents

The total ROS production was assessed using DCFH, with experimental results presented in Fig. 3. BDP-F Lips, BDP-Cl Lips and BDP-Br Lips all demonstrated robust ROS generation capacity, sustained ROS production over extended durations, and notable photostability. BDP-1 served as the control for comparing the enhanced PDT efficacy of BDP-F, BDP-Cl, and BDP-Br. After the introduction of various heavy atom groups, the ROS yield was significantly enhanced. For $O_2^{\bullet-}$ generation, BDP-1 exhibited the lowest production capacity, demonstrating that heavy atom group incorporation substantially improves Type II PDT output. Regarding singlet oxygen production, BDP-1 performed relatively well among the four photosensitizers, which is consistent with conventional photosensitizers. As shown in Fig. 3(D), BDP-F Lips exhibited the highest ROS yield, achieving a 17-fold increase after 360 s, attributable to three factors: I) Electronegativity disparity. Fluorine possesses the highest electronegativity (4.0) among halogens. Its strong electron-withdrawing capacity enhances polarization of the electron-accepting (A) unit within the photosensitizer through an inductive effect, facilitating charge separation and improving electron transfer efficiency. Conversely, chlorine (3.0) and bromine (2.8) exhibit lower electronegativities, resulting in weaker driving forces for electron transfer. II) Enhanced intersystem crossing (ISC). Fluorine's potent electron-accepting ability optimizes excited-state energy level distribution, prolongs triplet excited-state lifetime, and promotes energy transfer between the photosensitizer and oxygen. III) Atomic radius and molecular stacking. The smaller atomic radius of fluorine (0.64 Å) reduces steric hindrance upon substitution, enabling formation of closely packed aggregates. Such aggregation simultaneously suppresses fluorescence quenching while maintaining high ROS generation activity. In contrast, chlorine (0.99 Å) and bromine (1.14 Å) exhibit larger atomic

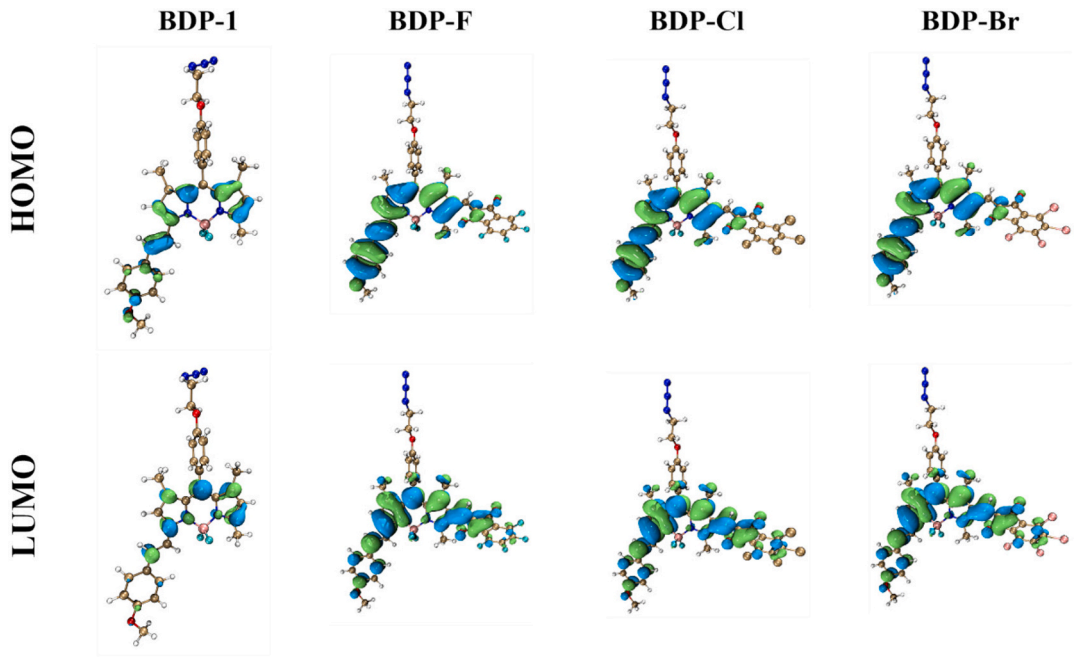

Fig. 2. Illustration of the frontier molecular orbitals of the HOMO and LUMO determined at the B3LYP/6-31G(d) level of theory, Gaussian 16 program.

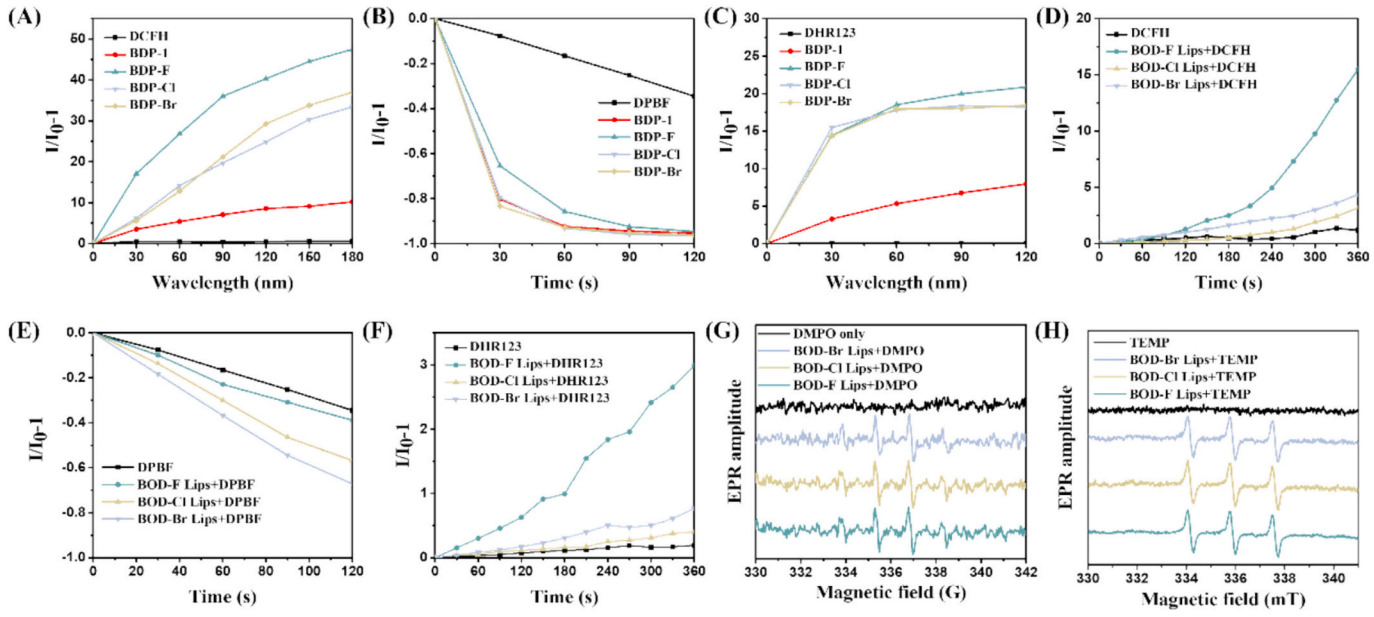

Fig. 3. Relative changes in PL intensity of (A) DCFH (for ROS generation), B) DHR-123 (for $O_2^{\bullet-}$ detection), C) DPBF (for $^1O_2$ detection) in the presence of 10 μM BDP-1, BDP-F, BDP-Cl and BDP-Br upon white light irradiation.
Relative changes in PL intensity of (D) DCFH (for ROS generation), E) DPBF (for $^1O_2$ detection) F) DHR-123 (for $O_2^{\bullet-}$ detection) in the presence of 10 μM BDP-F Lips, BDP-Cl Lips and BDP-Br Lips upon white light irradiation. G,H) EPR signals of BDP-F Lips, BDP-Cl Lips and BDP-Br Lips in PBS. White light: 20 mW cm^{-2}.

radii that may cause looser molecular packing and reduced ROS yields in aggregated states. Notably, BDP-Br Lips surpassed BDP-Cl Lips in ROS production despite bromine's lower electronegativity. This anomaly arises from: I) Augmented spin-orbit coupling. Bromine's substantially greater atomic mass versus chlorine and fluorine intensifies the heavy-atom effect, significantly promoting spin-orbit coupling. This enhances ISC efficiency, extends triplet excited-state lifetime, and thereby amplifies Type II ROS (singlet oxygen, $^1O_2$) generation. This interpretation aligns with Fig.S21 (ESI†) data. Although bromine exhibits weaker electron-withdrawing capacity than chlorine, its heavy-atom effect compensates for reduced electron transfer efficiency, yielding an overall higher ROS production. II) Atomic radius influence. Bromine's larger atomic radius causes slightly looser molecular packing yet maintains higher ROS yields through heavy-atom effects. Singlet oxygen detection using DPBF (Fig. 3(E)) revealed the following generation capacity order: BDP-Br Lips > BDP-Cl Lips > BDP-F Lips. This trend corroborates the analysis that heavier atoms induce stronger heavy-atom effects, enhance spin-orbit coupling, improve ISC efficiency, prolong triplet-state lifetime, and consequently boost Type II ROS ($^1O_2$) production. Superoxide radical detection via DHR123 (Fig. 3(F)) demonstrated the generation sequence: BDP-F Lips > BDP-Cl Lips > BDP-Br Lips. The core mechanism for Type I ROS (e.g., $O_2^{\bullet-}$) involves the inductive effect: higher

electronegativity strengthens electron-withdrawing capacity, intensifying polarization of the electron-accepting (A) unit within the photosensitizer. This promotes charge separation, enhances electron transfer efficiency, and ultimately increases Type I ROS generation. Electron paramagnetic resonance (EPR) spectroscopy was performed using TEMP as the $^1O_2$ spin trap and DMPO as the ·OH spin trap after a 10-min light irradiation of liposomal photosensitizers. Characteristic signals confirmed the generation of both singlet oxygen and hydroxyl radicals, demonstrating that all three liposomal photo-sensitizers concurrently produce Type I ROS (·OH) and Type II ROS ($^1O_2$).

ROS Generation in *E. coli* was evaluated using the DCFH-DA probe. As shown in Fig. 4(A), the mixture of BDP-F Lips and *E. coli* exhibited significantly stronger fluorescence intensity after white-light irradiation compared to the PBS control group and the non-irradiated mixture group. This demonstrates that BDP-F Lips efficiently generate ROS within bacterial, confirming their suitability for photodynamic antibacterial applications. The cytotoxicity of BDP-F Lips was investigated in 3 T3 cells using the CCK-8 assay. Prior to irradiation, all samples exhibited cell viability exceeding 98 %, confirming excellent biocompatibility. Post-irradiation, cellular survival rates decreased consistently across test groups, with the magnitude of reduction aligning quantitatively with ROS measurements (Fig. 4(B)). Post-irradiation viability remained above 90 %, with cells treated with 200 μg mL-1 of the photosensitizer liposomes retaining 91 % viability. These results confirmed the excellent cytocompatibility of BDP-F Lips.

Photodynamic therapy and antibacterial mechanism

Based on the priori results, we evaluated the in vitro antibacterial activities of three liposomal photosensitizers under both non-irradiated and irradiated conditions. As shown in Fig. 5, In the absence of light illumination, none of the three liposomal photosensitizers exhibited inhibitory effects against bacteria, with bacterial survival rates exceeding 95 %, confirming the absence of dark toxicity in all three formulations and establishing a foundation for subsequent in vivo studies. Following white light irradiation, all three photosensitizers demonstrated bacteriostatic effects against *E. coli*, with BDP-F Lips showing the most potent efficacy, consistent with the preceding ROS assay results. However, no significant antibacterial activity against *S. aureus* was observed for any photosensitizer, though a marginal reduction in colony count occurred in BDP-F Lips-treated samples. This differential efficacy may stem from structural differences between bacterial types: Gram-positive *S. aureus* possesses a thick (20–80 nm) peptidoglycan layer with negatively charged teichoic acids that creates electrostatic repulsion against negatively charged liposomes, preventing cellular proximity and hydrophobic disruption, while the dense peptidoglycan structure further impedes penetration of liposomes or ROS. In contrast, Gram-negative *E. coli*'s outer membrane contains densely packed, negatively charged LPS where local hydrophobic domains or auxiliary components (e.g., cholesterol) in liposomes may interact with LPS's lipid A moiety to compromise membrane integrity, and PDT-generated ROS can oxidize LPS fatty acid chains to enhance permeability. Due to its superior antibacterial performance, BDP-F Lips was selected as the representative model for investigating antimicrobial mechanisms. *E. coli* treated with BDP-F Lips were stained with SYTO 9 for green fluorescence marking live bacteria and PI for red fluorescence indicating dead bacteria, followed by observation using Fluorescence microscope (FM). Fig.S25 demonstrates that bacteria in both PBS control groups with and without light irradiation exhibited green fluorescence, indicating intact cellular structures. The BDP-F Lips-treated group without irradiation also displayed green fluorescence. In contrast, BDP-F Lips-treated samples exposed to white-light irradiation for merely five minutes showed distinct red fluorescence, proving damage to the *E. coli* cell membrane and consequent loss of bacterial viability. To further characterize bacterial morphology before and after treatment, scanning electron microscopy was employed. Fig.S26 reveals that untreated *E. coli* displayed typical rod-shaped morphology with smooth, undamaged surfaces, demonstrating healthy cellular architecture. Post-treatment samples exhibited significant morphological alterations including noticeable cellular lysis, rupture of cell walls and membranes, and exposure of internal structures. These observations confirm the potent bactericidal effect of BDP-F Lips against *Escherichia coli*. Integrating both experimental findings, we propose an antimicrobial mechanism by which BDP-F Lips generate reactive oxygen species under white-light irradiation to disrupt cellular membrane integrity, ultimately causing bacterial lysis and death.

In conclusion, three photosensitizers designed based on the push-pull electronic effect and heavy-atom effect were fabricated into liposomes via the thin-film hydration method, demonstrating favorable biocompatibility and low cytotoxicity with excellent application potential. In subsequent ROS assays, BDP-F Lips exhibited optimal ROS generation performance. All three liposomes simultaneously produced both Type I and Type II PDT, filling a gap in this research field. During antibacterial testing, BDP-F Lips displayed remarkable efficacy against *E. coli* by disrupting bacterial membrane integrity. This novel photosensitizer design strategy provides a new methodology for future research.

CRediT authorship contribution statement

Zhihua Chen: Writing – review & editing, Writing – original draft, Visualization, Validation, Project administration, Methodology, Investigation, Formal analysis, Data curation, Conceptualization. **Jincheng Zhu:** Data curation. **Mengxing Wang:** Data curation. **Qinglin Wu:** Data curation. **Yichun Xu:** Resources, Methodology. **Lei Cui:** Resources, Project administration, Methodology, Funding acquisition. **Kewen Zheng:** Resources, Funding acquisition.

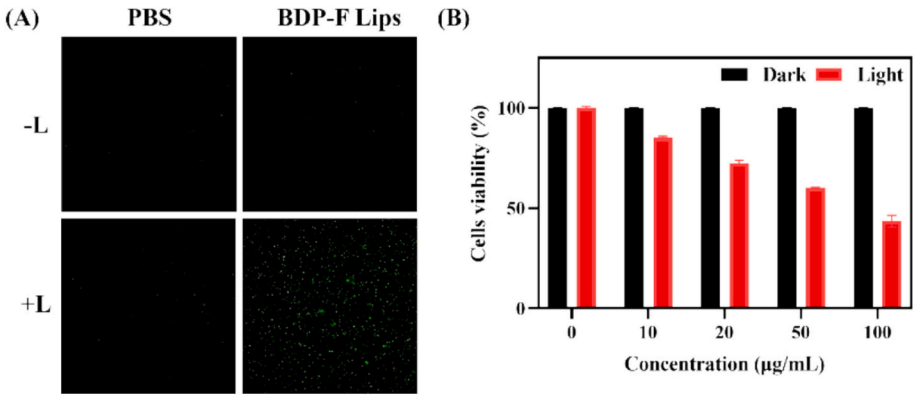

Fig. 4. (A) Intracellular ROS fluorescence images of *E. coli* incubated with PBS or BDP-F Lips (100 μg mL^{-1}) in the absence and presence of white light (5 min). (B) Cell viability of 3 T3 cells incubated with BDP-F Lips with different concentrations in the absence and presence of white light irradiation detected by CCK-8 assay.

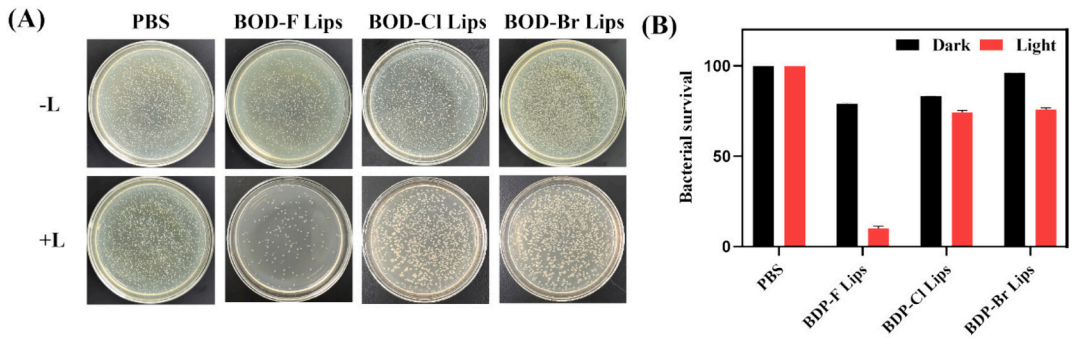

Fig. 5. (A) Representative images of *S. aureus* and *E. coli* colonies treated with three liposomal photosensitizers (10 mg mL^{-1}) under white light irradiation. (B) Corresponding bacterial survival rates.

Declaration of generative AI and AI-assisted technologies in the writing process

During the preparation of this work the authors used Deepseek in order to improve language. After using this tool, the authors reviewed and edited the content as needed and take full responsibility for the content of the publication.

Declaration of competing interest

The authors declare that they have no known competing financial interests or personal relationships that could have appeared to influence the work reported in this paper.

Acknowledgements

We thank the National Natural Science Foundation of China (Grant No. 82203232) for financial support.

Appendix A. Supplementary data

Supplementary data to this article can be found online at https://doi.org/10.1016/j.tetlet.2025.155830.

Data availability

No data was used for the research described in the article.

References

[1] J.A. Bartell, L.M. Sommer, J.A.J. Haagensen, A. Loch, R. Espinosa, S. Molin, H. K. Johansen, Evolutionary highways to persistent bacterial infection, Nat. Commun. 10 (1) (2019) 629.
[2] J.M. Franke, B.K. Raliski, S.C. Boggess, D.V. Natesan, E.T. Koretsky, P. Zhang, et al., BODIPY fluorophores for membrane potential imaging, J. Am. Chem. Soc. 141 (32) (2019) 12824–12831.
[3] P. Jagtap, V. Sritharan, S. Gupta, Nanotheranostic approaches for management of bloodstream bacterial infections, Nanomedicine 13 (1) (2017) 329–341.
[4] L.-Q. Ren, B. Zhan, J. Zhao, Y. Guo, B. Zu, Y. Li, C. He, Modular enantioselective assembly of multi-substituted boron-stereogenic BODIPYs, Nat. Chem. 17 (1) (2025) 83–91.
[5] H. Wei, L. Yang, C. Pang, L. Lian, L. Hong, Bacteria-targeted photothermal therapy for combating drug-resistant bacterial infections, Biomater. Sci. 11 (16) (2023) 5634–5640.
[6] N.J. Anyaegbunam, C.C. Anekpo, Z.K.G. Anyaegbunam, Y. Doowuese, C. B. Chinaka, O.J. Odo, et al., The resurgence of phage-based therapy in the era of increasing antibiotic resistance: from research progress to challenges and prospects, Microbiol. Res. 264 (2022) 127155.
[7] A. Eskenazi, C. Lood, J. Wubbolts, M. Hites, N. Balarjishvili, L. Leshkasheli, et al., Combination of pre-adapted bacteriophage therapy and antibiotics for treatment of fracture-related infection due to pandrug-resistant Klebsiella pneumoniae, Nat. Commun. 13 (1) (2022) 302.
[8] F. Molina, M. Menor-Flores, L. Fernández, M.A. Vega-Rodríguez, P. García, Systematic analysis of putative phage-phage interactions on minimum-sized phage cocktails, Sci. Rep. 12 (1) (2022) 2458.
[9] B.P. Lazzaro, M. Zasloff, J. Rolff, Antimicrobial peptides: application informed by evolution, Science 368(6490):eaau5480 (2020).
[10] M.N. Melo, R. Ferre, M.A.R.B. Castanho, Antimicrobial peptides: linking partition, activity and high membrane-bound concentrations, Nat. Rev. Microbiol. 7 (3) (2009) 245–250.
[11] D. Roversi, C. Troiano, E. Salnikov, L. Giordano, F. Riccitelli, M. De Zotti, et al., Effects of antimicrobial peptides on membrane dynamics: a comparison of fluorescence and NMR experiments, Biophys. Chem. 300 (2023) 107060.
[12] G. Feng, G.-Q. Zhang, D. Ding, Design of superior phototheranostic agents guided by Jablonski diagrams, Chem. Soc. Rev. 49 (22) (2020) 8179–8234.
[13] Q. Jia, Q. Song, P. Li, W. Huang, Rejuvenated photodynamic therapy for bacterial infections, Adv. Healthc. Mater. 8 (14) (2019) 1900608.
[14] V.-N. Nguyen, Y. Yan, J. Zhao, J. Yoon, Heavy-atom-free photosensitizers: from molecular design to applications in the photodynamic therapy of Cancer, Acc. Chem. Res. 54 (1) (2021) 207–220.
[15] R.L. Gapare, A. Thompson, Substitution at boron in BODIPYs, Chem. Commun. 58 (53) (2022) 7351–7359.
[16] S. Zhen, Z. Xu, M. Suo, T. Zhang, M. Lyu, T. Li, et al., NIR-II AIE liposomes for boosting type-I photodynamic and mild-temperature Photothermal therapy in breast Cancer treatment, Adv. Mater. 37 (3) (2025) 2411133.
[17] W. Wang, T. Qin, H. Wang, Z. Yang, Z. Chi, X. Zhou, Asymmetric A-DA'D-A″ molecular configuration type-I photosensitizer with two complementary reactive oxygen species for efficient imaging and photodynamic therapy, Adv Opt Mater 12 (2) (2024) 2301403.
[18] Z. Wang, Y. Xie, K. Xu, J. Zhao, K.D. Glusac, Diiodobodipy-styrylbodipy dyads: preparation and study of the intersystem crossing and fluorescence resonance energy transfer, J. Phys. Chem. A 119 (26) (2015) 6791–6806.